

Current-driven inertial domain wall dynamics in ferromagnet

Zai-Dong Li(李再东)

Citation: Chin. Phys. B, 2025, 34 (**10**): 107513. DOI: 10.1088/1674-1056/adfbd7
http://cpb.iphy.ac.cn; http://iopscience.iop.org/cpb

What follows is a list of articles you may be interested in

Deformation of magnetic skyrmion due to skyrmion-skyrmion interaction

Zhen-Qian Cui(崔振茜), Wen-Li Yang(杨文力), and Jun-Hui Zheng(郑俊辉)
Chin. Phys. B, 2025, 34 (**7**): 077502. DOI: 10.1088/1674-1056/adca20

Bifurcation of the bound states in the continuum in a dissipative cavity magnonic system

Xinlin Mi(米锌林), Lijun Yan(闫丽君), Bimu Yao(姚碧霖), Shishen Yan(颜世申), Jinwei Rao(饶金威), and Lihui Bai(柏利慧)
Chin. Phys. B, 2025, 34 (**6**): 067508. DOI: 10.1088/1674-1056/add4e4

Direct observation of ultrafast magnetization dynamics in Co/Ni bit patterned media by time-resolved scanning Kerr microscopy

Wei Zhang(张伟), Wei He(何为), Qin-Li Lv(吕琴丽), Jian-Wang Cai(蔡建旺), Xiang-Qun Zhang(张向群), and Zhao-Hua Cheng(成昭华)
Chin. Phys. B, 2025, 34 (**4**): 047501. DOI: 10.1088/1674-1056/adb67e

Inertial effect on minimum magnetic field for magnetization reversal in ultrafast magnetism

Xue-Meng Nan(南雪萌), Chuan Qu(屈川), Peng-Bin He(贺鹏斌), and Zai-Dong Li(李再东)
Chin. Phys. B, 2023, 32 (**12**): 127506. DOI: 10.1088/1674-1056/acd3de

Domain wall dynamics in magnetic nanotubes driven by an external magnetic field

Zai-Dong Li(李再东), Yue-Chuan Hu(胡月川), Peng-Bin He(贺鹏斌), Lin-Lin Sun(孙琳琳)
Chin. Phys. B, 2018, 27 (**7**): 077505. DOI: 10.1088/1674-1056/27/7/077505

SPECIAL TOPIC — Advanced magnonics

Current-driven inertial domain wall dynamics in ferromagnet

Zai-Dong Li(李再东)[†]

Tianjin Key Laboratory of Quantum Optics and Intelligent Photonics, School of Science, Tianjin University of Technology, Tianjin 300384, *China*
School of Mathematics and Physics, Xinjiang Hetian College, Hetian 848000, *China*

(Received 21 June 2025; revised manuscript received 10 August 2025; accepted manuscript online 15 August 2025)

We investigate the inertial domain wall (DW) dynamics driven by spin-polarized current in ferromagnets. The exact solutions reveal an upper limit for DW velocity, given by $V \leq 1/\sqrt{\alpha\tau}$. This indicates that damping and inertia become the key factors in achieving higher DW speeds. For the case of uniaxial anisotropy, we analyze the effects of inertia and current on DW dynamics. Due to inertia, the DW velocity, width, rotation frequency, and wave number are mutually coupled. When the DW width varies slightly, the velocity decreases rapidly while the magnetization precession frequency increases sharply with the inertia term. However, once the rotation frequency exceeds its maximum value, both the DW velocity and rotation frequency gradually decline. Regarding current-driven dynamics, we identify a critical current j_{1c} that directly triggers the Walker breakdown. For currents below this threshold $j_1 < j_{1c}$, the absolute DW velocity increases with current, whereas it decreases for $j_1 > j_{1c}$. During this process, the DW velocity rapidly peaks under current drive, accompanied by the magnetization rotation frequency nearing its maximum and minimal variation in DW width. These results suggest that the DW behaves like a classical rigid body, reaching its maximum velocity as it approaches peak rotational speed. For biaxial anisotropy, we derive analytical solutions. The competition between hard-axis anisotropy and inertia causes the DW magnetization to lose its spiral structure and rotational symmetry. The inertia effect leads to a slow initial decrease followed by a rapid increase in DW width, whereas current modulation gradually widens the DW. The analytical solution also reveals another critical current, $j_{1\max} = \sqrt{\alpha/\tau}/\beta$, which scales with the square root of the inertia-to-damping ratio and is inversely proportional to the nonadiabatic spin-transfer torque parameter β.

Keywords: inertial effect, ultrafast magnetism, domain wall dynamics

PACS: 75.78.–n, 71.70.Ej, 72.25.Rb

DOI: 10.1088/1674-1056/adfbd7 **CSTR:** 32038.14.CPB.adfbd7

1. Introduction

Spin dynamics serves as the cornerstone for advancing next-generation spintronic and magnetoelectronic technologies. Pioneering experiments on magnetic materials at sub-picosecond and femtosecond timescales have revolutionized our fundamental understanding of ultrafast magnetic phenomena. These landmark studies conclusively established that the conventional Landau–Lifshitz–Gilbert (LLG) equation, formulated originally for nanosecond-scale spin precession, can be generalized to include inertial effects through the introduction of spin nutation dynamics at sub-picosecond and femtosecond timescales.[1–12] Building upon this inertial LLG (ILLG) framework, the research community has developed a comprehensive theoretical foundation for magnetization nutation phenomena, encompassing nutation spectroscopy, resonant nutation behavior, inertial spin dynamics, and their connection to quantum Brownian motion.[13–23]

Magnetic domains, serving as fundamental units for information storage, have garnered significant attention due to the ultrafast motion capabilities of magnetic domain walls (DWs) in next-generation high-speed information storage and processing systems. Current research demonstrates three primary approaches for DW manipulation: magnetic field-driven motion,[24,25] spin-polarized current-induced propagation,[26–30] and a combination of field-current-driven motion,[31,32] all of which enable DWs to overcome pinning potentials and propagate through magnetic nanowires. From a fundamental standpoint, the analytical solutions for DW dynamics under various driving mechanisms provide particularly valuable physical insights. The classical Walker solution[33] first established an exact description for field-driven DWs in easy-axis ferromagnets, while Berger's pioneering work[26,27] revealed that spin-polarized currents exert exchange-mediated forces and introduce novel magnetization torques.[34,35] Crucially, unlike magnetic fields, spin-polarized currents enable ultrafast magnetization switching,[36] offering distinct advantages for nanoscale devices, including simplified fabrication and reproducible high-speed operation.[37,38]

Interestingly, the coupling between spins and other degrees of freedom has been shown to induce effective inertia in spin dynamics within ferromagnetic materials,[16–18,39–41] and experimental evidence has confirmed the existence of nutational spin dynamics in such systems. On femtosecond timescales, spin inertia[19,20,42] must be explicitly taken into

[†]Corresponding author. E-mail: lizd@email.tjut.edu.cn

© 2025 Chinese Physical Society and IOP Publishing Ltd. All rights, including for text and data mining, AI training, and similar technologies, are reserved.

account. A theoretical framework has been developed to describe precession self-oscillations in ferromagnetic materials with spin inertia, where nutation self-oscillations may play a crucial role in future ultra-high-frequency technologies.[43] Moreover, the ILLG equation predicts that inertial effects can enhance the propagation velocity of field-driven DWs.[44]

Despite significant advances in ultrafast spin dynamics research, investigations into spin inertia remain in their early stages. In this work, we incorporate inertial effects with spin-transfer torque[45–52] to control magnetization dynamics, establishing a theoretical framework for current-driven DW motion in ferromagnetic systems.

2. Model

As a model system, we consider a biaxial anisotropic ferromagnet with the easy axis (z axis) oriented perpendicular to the wire axis (x axis). The magnetization dynamics is governed by the dimensionless ILLG equation incorporating spin-transfer torque effects[7,8,15,19,20,34,35,40,53,54]

$$\begin{aligned}\dot{\boldsymbol{m}} &= -\boldsymbol{m}\times\boldsymbol{h}_{\rm eff}+\alpha\boldsymbol{m}\times\dot{\boldsymbol{m}}-j_1\partial\boldsymbol{m}\\ &\quad+\beta j_1\boldsymbol{m}\times\partial\boldsymbol{m}+\alpha\tau\left(\boldsymbol{m}\times\ddot{\boldsymbol{m}}\right),\end{aligned}\tag{1}$$

where $\boldsymbol{m}$ is the normalized magnetization, $\boldsymbol{m}\equiv\boldsymbol{M}/M_{\rm s}$, $\boldsymbol{M}$ is the localized magnetization with $M_{\rm s}$ being the saturation magnetization, $\dot{\boldsymbol{m}}$ represents the derivative with respect to time t, and the definitions $\partial\equiv\partial/\partial x$ and $\partial^2\equiv\partial^2/\partial x^2$ are adopted, where the time $t(\tau)$ and space coordinate x are rescaled by the characteristic time $t_0=1/(\gamma M_{\rm s})$ and length $x_0=\sqrt{J_0/(\mu_0 M_{\rm s}^2)}$, respectively. Here, γ is the gyromagnetic ratio, J_0 is the exchange constant, and μ_0 is the vacuum permeability. The dimensionless effective field is given by $\boldsymbol{h}_{\rm eff}=\partial^2\boldsymbol{m}/\partial x^2+\kappa_3 m_3\boldsymbol{e}_z-\kappa_1 m_1\boldsymbol{e}_x$, with $\kappa_3=K_3/\left(\mu_0 M_{\rm s}^2\right)$, $\kappa_1=K_1/\left(\mu_0 M_{\rm s}^2\right)$, where κ_3 is the easy-axis anisotropy parameter, and κ_1 is the hard-axis anisotropy parameter. In Eq. (1), the second term on the right-hand side describes the damping effect characterized by the Gilbert damping parameter α. The third and fourth terms represent the adiabatic and nonadiabatic spin-transfer torques, respectively, where $j_1=J_1 P\mu_{\rm B}/(eM_{\rm s})$ denotes the dimensionless current density,[34,55] where P is the spin polarization of the current, $\mu_{\rm B}$ is the Bohr magneton, and e is the electron charge. The final term accounts for the effect of magnetization inertia, where τ is the angular momentum relaxation time that induces spin nutation analogous to the nutational motion of a symmetric spinning top. Specifically, within certain energy regimes, the axis of the top undergoes simultaneous precession about the field direction and oscillatory nutational motion.[17]

In spherical coordinates $\left\{\boldsymbol{e}_r,\boldsymbol{e}_\theta,\boldsymbol{e}_\varphi\right\}$, with $\boldsymbol{m}=(1,0,0)$, we have $\dot{\boldsymbol{m}}=\dot\theta\boldsymbol{e}_\theta+\dot\phi\sin\theta\boldsymbol{e}_\phi$, and $\partial\boldsymbol{m}=\partial\theta\boldsymbol{e}_\theta+\sin\theta\partial\phi\boldsymbol{e}_\phi$. Substituting these into Eq. (1), we obtain

$$\begin{aligned}\dot\theta+\alpha\dot\phi\sin\theta &= \sin\theta\left(\partial^2\phi-\frac{\kappa_1}{2}\sin 2\phi-\beta j_1\partial\phi\right)\\ &\quad+2\cos\theta\left(\partial\theta\partial\phi-\alpha\tau\dot\theta\dot\phi\right)\\ &\quad-j_1\partial\theta-\alpha\tau\ddot\phi\sin\theta,\end{aligned}\tag{2}$$

$$\begin{aligned}\dot\phi\sin\theta-\alpha\dot\theta &= \frac{1}{2}\sin 2\theta\left[(\partial\phi)^2+\kappa_3+\kappa_1\cos^2\phi-\alpha\tau\dot\phi^2\right]\\ &\quad-\partial^2\theta+\alpha\tau\ddot\theta-j_1(\sin\theta\partial\phi-\beta\partial\theta),\end{aligned}\tag{3}$$

in which the spatial and temporal parameters θ and ϕ are defined by $\boldsymbol{m}\equiv(\sin\theta\cos\phi,\sin\theta\sin\phi,\cos\theta)$. In the subsequent analysis, we will systematically examine inertial DW dynamics for both uniaxial and biaxial anisotropy cases.

2.1. Exact inertial DW dynamics for uniaxial anisotropy

In this section, we focus specifically on the uniaxial anisotropy case ($\kappa_1=0$). The exact analytical solution describing inertial DW dynamics with spiral configuration is given by

$$\begin{aligned}\theta &= 2\arctan{\rm e}^{(x-Vt)/\Delta},\\ \phi &= \omega t-\Gamma x+\phi_0,\end{aligned}\tag{4}$$

where

$$V=\frac{\Delta}{\alpha_1}\left(a_2\Gamma-a_1/\Delta\right),\tag{5}$$

$$\omega=\frac{1}{\alpha_1}\left(a_1\Gamma+a_2/\Delta\right),\tag{6}$$

$$\Gamma=-\alpha\tau V\omega,\tag{7}$$

$$\Delta=\Delta_0\sqrt{f_0/\left(1-f_0\alpha\tau\omega^2\Delta_0^2\right)},\tag{8}$$

with $\alpha_1=1+\alpha^2$, $a_1=-j_1(1+\alpha\beta)$, $a_2=-j_1(\alpha-\beta)$, $\Delta_0=1/\sqrt{\kappa_3}$, and $f_0=1-\alpha\tau V^2$. From Eqs. (5)–(8), we first recover the DW dynamic properties in fast magnetism, i.e., $\tau=0$, which gives $\Gamma=0$, $\Delta=\Delta_0=1/\sqrt{\kappa_3}$, $V=j_1(1+\alpha\beta)/\alpha_1$, and $\omega=-j_1(\alpha-\beta)\sqrt{\kappa_3}/\alpha_1$. These results clearly indicate that the DW velocity V, DW width Δ, rotation frequency ω, and wave number Γ are mutually independent. However, this apparent independence does not hold in ultrafast magnetization dynamics, where these intrinsic DW parameters are mutually coupled, as evidenced by Eqs. (5)–(8). By decoupling the four equations we obtain

$$\omega=\frac{a_2}{f_1\Delta_0},\tag{9}$$

$$V=\frac{\alpha_1}{2\alpha\tau a_1}\left[-b_1+\sqrt{b_1^2-4\alpha\tau\left(a_1/\alpha_1\right)^2}\right],\tag{10}$$

where $f_1=\sqrt{f_0\left(\alpha_1+\alpha\tau a_1 V\right)^2+\alpha\tau a_2^2}$ and $b_1=1+\alpha\tau j_1^2\left(1+\beta^2\right)$. So, from Eqs. (7) and (8) we can obtain the analytical form of wave number Γ and DW width Δ with Eqs. (9) and (10), respectively.

Under inertial effects, DW dynamics exhibit novel excitation modes, as demonstrated in Eqs. (9) and (10). First,

when $\tau \to 0$, the DW velocity V recovers the conventional fast-magnetism behavior. Equation (10) reveals an inverse dependence of DW velocity on inertial parameter τ, as illustrated in Fig. 1(a). Notably, the constraint $f_0 \geq 0$ imposes an upper bound on the DW velocity: $V \leq 1/\sqrt{\alpha\tau}$. This maximum velocity $V_{\max} = 1/\sqrt{\alpha\tau}$ shows an inverse square-root dependence on both inertia and damping parameters, suggesting that damping, quantified by $1/\sqrt{\alpha}$, becomes the dominant factor in achieving higher DW propagation speeds. Second, inertial effects induce non-monotonic variations in both precession frequency $|\omega|$ and wave number Γ, displaying characteristic initial increases followed by decreases, as shown in Figs. 1(b) and 1(c). While the Dzyaloshinskii–Moriya interaction (DMI) is known to stabilize spiral magnetization configurations,[55] Eq. (7) demonstrates that inertia alone can excite spiral DW structures in uniaxial anisotropic ferromagnets,[44] even in the absence of DMI. Finally, the DW width exhibits an opposite trend, initially decreasing but then undergoing rapid expansion, as shown in Fig. 1(d).

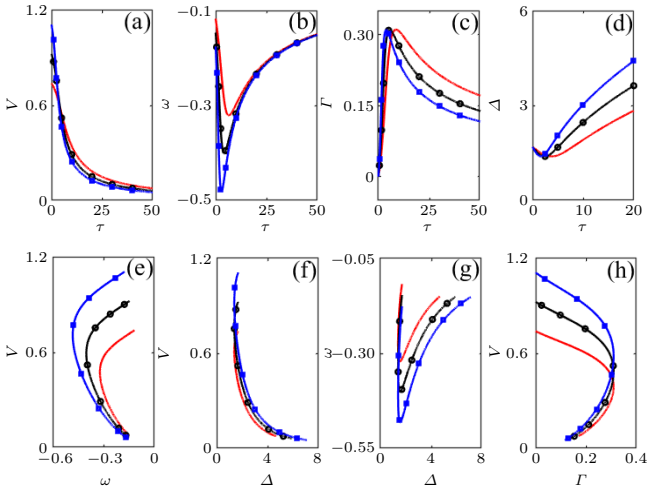


Fig. 1. The inertial effect on the DW velocity V in (a), frequency ω in (b), wave number Γ in (c), and DW width Δ in (d) for the case of uniaxial ferromagnet. (e)–(h) The corresponding relationships between V and ω, V and Δ, ω and Δ, and V and Γ at the same moment. The parameters are $\alpha = 0.3$, $\beta = 0.03$, $\kappa_3 = 0.35$, and $j_1 = 0.8$, 1.0, 1.2, which are shown by the red line, the short black dotted line, and the long blue dotted line, respectively.

To elucidate the correlation between the intrinsic characteristics of DW dynamics, we present a systematic analysis in Figs. 1(e)–1(h). Under the action of inertial effects, the DW velocity exhibits a rapid decrease while the DW width shows minimal variation with increasing magnetization rotation frequency, as shown in Figs. 1(e) and 1(f). Figures 1(f) and 1(g) demonstrate that, when the DW width remains nearly constant, the DW velocity decreases sharply while the magnetization precession frequency increases rapidly. Notably, once the rotation frequency surpasses its maximum value, both the DW velocity and rotation frequency display a gradual decline, as shown in Figs. 1(e)–1(g). Figure 1(h) presents the coevolution of DW velocity and wave number, revealing that the spin wave number induced by magnetization precession first decreases rapidly and then recovers slowly, providing a clear manifestation of inertial modulation on the spatial phase.

We systematically investigate the impact of spin-polarized current on inertial DW dynamics in uniaxial anisotropic ferromagnets. For the non-inertial case ($\tau = 0$), both the DW velocity $V = j_1(1+\alpha\beta)/\alpha_1$ and rotation frequency $\omega = -j_1(\alpha-\beta)\sqrt{\kappa_3}/\alpha_1$ exhibit linear proportionality to the current density j_1, as indicated by the red curves in Figs. 2(a) and 2(b). Remarkably, introducing inertia ($\tau \neq 0$) reveals a critical current density $j_{1c} = 1/\sqrt{\alpha\tau(1+\beta^2)} = V_{\max}/\sqrt{1+\beta^2}$ that triggers the current-induced Walker breakdown. This establishes a fundamental relationship between the maximum DW velocity and the driving current in uniaxial anisotropic systems, where the critical DW velocity is $V_c \approx V_{\max}$. As demonstrated in Fig. 2(a), the system displays distinct dynamic regimes: below this critical threshold $j_1 < j_{1c}$, the absolute DW velocity increases monotonically with current, whereas above the threshold $j_1 > j_{1c}$, the velocity decreases with increasing current.

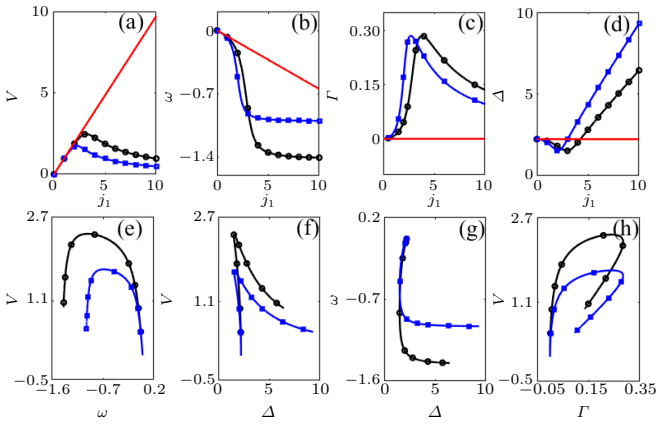


Fig. 2. The effect of external current on the DW velocity V in (a), frequency ω in (b), wave number Γ in (c), and DW width Δ in (d) for the case of a uniaxial ferromagnet. Curves for $\tau = 0$, 0.5, 1.0 are shown by the red line, the short black dotted line, and the long blue dotted line, respectively. (e)–(h) The corresponding relationships between V and ω, V and Δ, ω and Δ, and V and Γ at the same moment, where curves for $\tau = 0.5$ and 1.0 are shown by the short black dotted line and the long blue dotted line, respectively. The other parameters are $\alpha = 0.2$, $\beta = 0.05$, and $\kappa_3 = 0.2$.

When inertia is absent ($\tau = 0$), the wave number Γ vanishes while the DW width reduces to $\Delta_0 = 1/\sqrt{\kappa_3}$, as indicated by the red lines in Figs. 2(c) and 2(d). Notably, both the rotation frequency and wave number exhibit a rapid initial increase with current before gradually saturating, as illustrated in Figs. 2(b) and 2(c). Meanwhile, the current effectively modulates both Γ and Δ, with Figs. 2(c) and 2(d) showing a characteristic trend where the DW width first decreases and then increases again. This behavior is further confirmed in the large-current limit, where the DW velocity approaches $V \to 0$, the frequency tends to $|\omega| \to 1/\left(\sqrt{\alpha\tau}\Delta_0\right)$, and $\Gamma \to 1/\Delta_0$. Particularly intriguing is the result that under these conditions,

the rotational velocity ω/Γ of magnetization exactly matches the DW velocity V, with both converging to $1/\sqrt{\alpha\tau}$.

We now clarify the intrinsic relationships among V, ω, Γ, and Δ, as depicted in Figs. 2(e)–2(h). Under the ultrafast magnetics mechanism, the DW velocity rapidly accelerates to its maximum value when driven by the spin-polarized current, while the magnetization rotation frequency simultaneously approaches its peak value with minimal variation in DW width, as shown in Figs. 2(e)–2(g). This behavior suggests that the DW resembles a classical rigid body, reaching its maximum translational velocity when its rotational speed peaks. During this propagation process, the wave number Γ exhibits a non-monotonic variation, i.e., initially increasing and then decreasing, as shown in Fig. 2(h). This clearly demonstrates the dual role of spin-polarized current in both exciting and modulating the spin wave density (see supplementary material video 1 of DW dynamics).

Finally, Eqs. (7)–(10) reveal that DW motion is also influenced by the parameters α, β, and κ_3. The DW velocity is independent of κ_3, while the precession frequency, wave number, and width increase monotonically with κ_3. To illustrate the dependence of DW motion on α and β more clearly, we present the results in Fig. 3. Within the experimentally relevant parameter range, damping suppresses DW velocity, whereas spin-transfer torque enhances it, as shown in Figs. 3(a) and 3(e). In addition, damping leads to non-monotonic variations in the precession frequency, wave number, and width (Figs. 3(b)–3(d)), while spin-transfer torque produces monotonic changes in these quantities (Figs. 3(f)–3(h)).

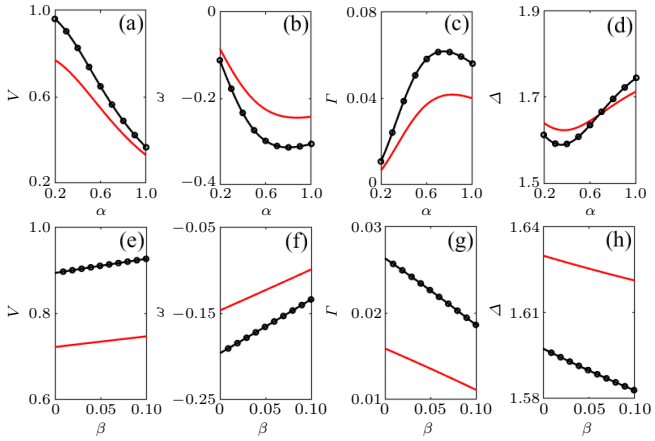


Fig. 3. (a)–(d) The effect of damping on the DW velocity V, frequency ω, wave number Γ, and DW width Δ, with parameter $\beta = 0.03$. (e)–(h) The effect of anisotropy on V, ω, Γ, and Δ, with parameter $\alpha = 0.3$. The other parameters are $\kappa_3 = 0.35$, $\tau = 0.5$, and $j_1 = 0.8$, 1.0, which are shown by the red line and the short black dotted line, respectively.

2.2. Inertial effect on DW dynamics for biaxial anisotropy

We now investigate inertial effects on DW dynamics in biaxial anisotropy ferromagnets ($\kappa_1 \neq 0$), where the exact inertial DW solution takes the form

$$\phi = \tfrac{1}{2}\arcsin\left(2a_3/\Delta\right), \tag{11}$$

$$\theta = 2\arctan \mathrm{e}^{(x-Vt)/\Delta}, \tag{12}$$

with parameters

$$V = j_1\beta/\alpha, \tag{13}$$

$$\Delta = \sqrt{f_0/\left(\kappa_3 + \kappa_1\cos^2\phi\right)}, \tag{14}$$

where

$$\begin{aligned} a_3 &= a_2/\left(\alpha\kappa_1\right), \\ \cos^2\phi &= \left[\left(1 - a_3^2\kappa_1/f_0\right)\right. \\ &\quad \left.\pm\sqrt{\left(1 - a_3^2\kappa_1/f_0\right)^2 - 4a_3^2\kappa_3/f_0}\right]/2, \end{aligned}$$

and the parameter f_0 is defined in the previous section.

Equation (14) gives two distinct solutions corresponding to the "$\pm$" cases in $\cos^2\phi$. To clarify this dichotomy, we first consider $j_1 = 0$ ($a_3 = 0$), where the static equilibrium DW solutions from Eqs. (11) and (12) yield $\phi_0 = 0, \pi$ (i.e., $\cos\phi = \pm 1$). In this case, the "+" branch corresponds to the minimum-energy configuration — the stable static DW solution ($\phi = 0, \pi$, $\theta = 2\arctan \mathrm{e}^{x/\Delta}$), while the "−" branch corresponds to a saddle point ($\phi = \pi/2, 3\pi/2$, $\theta = 2\arctan \mathrm{e}^{x/\Delta}$), representing an unstable magnetic state. In the following, we restrict our analysis to the stable "+" solution.

Because of the competition between hard-axis anisotropy and inertia, spiral magnetization structures in DWs vanish ($\Gamma = 0$). While inertia tends to favor spiral configurations (lower-energy magnetic states), the hard-axis anisotropy enforces higher-energy alignments, ultimately suppressing spirals. As a result, the magnetization becomes pinned, and its rotational dynamics disappear ($\omega = 0$).

In biaxial anisotropy ferromagnets, Eq. (13) shows that the DW velocity is directly proportional to the current j_1 and controlled by both the nonadiabatic spin-transfer torque parameter β and the damping constant α. Figure 4(a) shows that increasing the inertial factor τ leads to an initial slow decrease of DW width, followed by a rapid expansion. By contrast, spin-polarized current broadens the DW width, as illustrated in Fig. 3(b).

The natural constraint

$$\left(1 - a_3^2\kappa_1/f_0\right)^2 - 4a_3^2\kappa_3/f_0 \geq 0$$

defines a critical current window $j_{1,-} \leq j_1 \leq j_{1+}$, where

$$j_{1,\pm} = \pm\frac{\xi_-}{\left(1-\beta/\alpha\right)\sqrt{1+\alpha\tau\alpha_2^2\xi_-^2}},$$

with $\xi_- = \sqrt{\kappa_3+\kappa_1} - \sqrt{\kappa_3}$ and $\alpha_2 = -\beta/\left(\alpha-\beta\right)$.

In addition, the condition $f_0 \geq 0$ sets the maximum DW velocity

$$V_{\max} = 1/\sqrt{\alpha\tau},$$

which scales inversely with the square roots of both inertia and damping. Remarkably, in this regime the damping factor α becomes the dominant parameter governing DW mobility through its $1/\sqrt{\alpha}$ dependence. When V approaches $V_{\max}$, the maximum driving current reaches

$$|j_{1\max}| = \sqrt{\alpha/\tau}/\beta,$$

which exactly coincides with the asymptotic limit $|j_{1,+}| \to \sqrt{\alpha/\tau}/\beta$ at large τ (see supplementary material video 2 of DW dynamics).

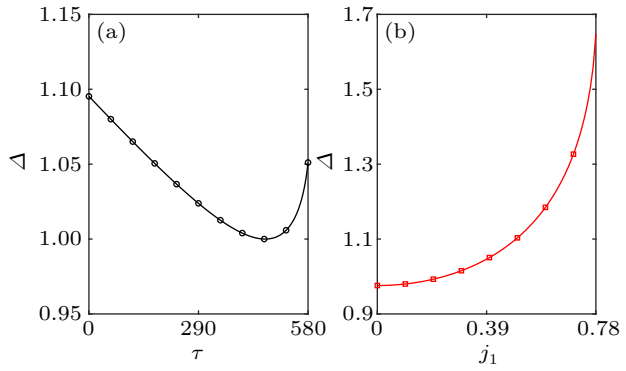


Fig. 4. The variation of DW width Δ as a function of the inertia parameter τ and the external current j_1 for the biaxial ferromagnet. (a) Parameters are $\alpha = 0.3$, $\beta = 0.03$, $\kappa_1 = 0.9$, $\kappa_3 = 0.2$, and $j_1 = 0.5$. (b) Parameters are $\alpha = 0.3$, $\beta = 0.03$, $\kappa_1 = 0.95$, $\kappa_3 = 0.1$, and $\tau = 5$.

3. Conclusion

Through our investigation of ultrafast magnetic phenomena, we have elucidated the fundamental characteristics of domain wall (DW) dynamics in both uniaxial and biaxial anisotropic ferromagnets under the combined influence of inertial effects and spin-transfer torque. By employing physically justified assumptions, we derived two exact analytical solutions for DW motion. These solutions demonstrate the existence of an intrinsic upper limit for DW velocity and reveal that the damping parameter, rather than other factors, emerges as the dominant determinant for achieving higher DW speeds.

In uniaxial anisotropic systems, we show that inertial effects induce coupled dynamics among DW velocity, width, rotation frequency, and wave number, while these quantities vary independently in the absence of inertia. Remarkably, the DW velocity can decrease rapidly while the magnetization precession frequency increases sharply, even with minimal variation in DW width. Beyond a threshold rotation frequency, both the velocity and frequency gradually decay. Under spin-polarized current driving, inertial DW dynamics exhibits several novel features. Most notably, we identify a critical current value that triggers current-induced Walker breakdown. When the applied current deviates from this critical value (either below or above), the system displays either positive or negative mobility. A particularly intriguing observation is that DW velocity can rapidly saturate to its maximum value under current driving, accompanied by near-simultaneous saturation of the magnetization rotation frequency with negligible change in wall width. This behavior suggests quasi-rigid-body motion, where translational velocity peaks precisely when rotational velocity reaches its maximum.

In biaxial anisotropic systems, the competition between hard-axis anisotropy and inertia leads to the disappearance of spiral magnetization structures and rotational characteristics in DWs. The DW width exhibits a non-monotonic dependence on the inertial parameter τ, initially decreasing slowly before undergoing rapid expansion. Conversely, current injection induces progressive broadening of the DW width. Our analysis reveals a critical current density

$$j_{1\max} = \sqrt{\alpha/\tau}/\beta,$$

demonstrating square-root dependence on the inertia–damping ratio α/τ and inverse proportionality to the nonadiabatic spin-transfer torque parameter β. This finding naturally raises the important question of experimental control of inertia.

Recent studies suggest that the angular momentum relaxation time τ can be optically modulated[56,57] or controlled via x-ray[58,59] techniques, with measured values reaching 72 ps in CoFeB systems.[19] Notably, the interplay between inertial effects and spin-polarized currents enables dynamic control of both spatial phase profiles and spin-wave densities, thereby offering precise manipulation of DW dynamics. To apply the theoretical model and results presented in this work for targeted prediction, we adopt the material parameters of NiFe: $\alpha = 0.1$, $\gamma = 2.21 \times 10^5$ A/(m·s), $\mu_0 = 4\pi \times 10^{-7}$ N/A^2, $J_0 = 1.3 \times 10^{-11}$ J/m, $M_s = 8 \times 10^5$ A/m, and $K_3 = 2.0 \times 10^5$ J/m^3. Therefore, the characteristic time, length, and velocity are obtained as $t_0 = 5.66 \times 10^{-12}$ s, $x_0 = 4.02 \times 10^{-9}$ m, and $v_0 \equiv x_0/t_0 = 710.83$ m/s, respectively. We further obtain the maximum speed $v_{\max} = 3198.74$ m/s at $\tau = 0.5$. These results establish a theoretical framework for spintronic device applications while creating new opportunities for achieving ultrafast magnetization reversal.

Acknowledgments

This work was supported by the Program of State Key Laboratory of Quantum Optics and Quantum Optics Devices, Shanxi University, China (Grant No. KF202203) and the Tianjin Natural Science Foundation Project (Grant No. 25JCQNJC00990).

References

[1] Ciornei M C, Rubi J M and Wegrowe J E 2011 *Phys. Rev. B* **83** 020410
[2] Fähnle M, Steiauf D and Illg C 2011 *Phys. Rev. B* **84** 172403
[3] Wegrowe J E and Ciornei M C 2012 *Am. J. Phys.* **80** 607

[4] Bhattacharjee S, Nordström L and Fransson J 2012 *Phys. Rev. Lett.* **108** 057204
[5] Olive E, Lansac Y and Wegrowe J E 2012 *Appl. Phys. Lett.* **100** 192407
[6] Böttcher D and Henk J 2012 *Phys. Rev. B* **86** 020404
[7] Kikuchi T and Tatara G 2015 *Phys. Rev. B* **92** 184410
[8] Olive E, Lansac Y, Meyer M, Hayoun M and Wegrowe J E 2015 *J. Appl. Phys.* **117** 213904
[9] Wegrowe J E and Olive E 2016 *J. Phys. Condens. Matter* **28** 106001
[10] Thonig D, Eriksson O and Pereiro M 2017 *Sci. Rep.* **7** 931
[11] Mondal R, Berritta M, Nandy A K and Oppeneer P M 2017 *Phys. Rev. B* **96** 024425
[12] Mondal R, Berritta M and Oppeneer P M 2018 *J. Phys. Condens. Matter* **30** 265801
[13] Li Y, Naletov V V, Klein O, Prieto J L, Muñoz M, Cros V, Bortolotti P, Anane A, Serpico C and de Loubens G 2019 *Phys. Rev. X* **9** 041036
[14] Giordano S and Déjardin P M 2020 *Phys. Rev. B* **102** 214406
[15] Titov S V, Coffey W T, Kalmykov Y P and Zarifakis M 2021 *Phys. Rev. B* **103** 214444
[16] Cherkasskii M, Farle M and Semisalova A 2020 *Phys. Rev. B* **102** 184432
[17] Titov S V, Coffey W T, Kalmykov Y P, Zarifakis M and Titov A S 2021 *Phys. Rev. B* **103** 144433
[18] Neeraj K, Pancaldi M, Scalera V, Perna S, d'Aquino M, Serpico C and Bonetti S 2022 *Phys. Rev. B* **105** 054415
[19] Neeraj K, Awari N, Kovalev S, *et al.* 2021 *Nat. Phys.* **17** 245
[20] Unikandanunni V, Medapalli R, Asa M, Albisetti E, Petti D, Bertacco R, Fullerton E E and Bonetti S 2022 *Phys. Rev. Lett.* **129** 237201
[21] Cherkasskii M, Barsukov I, Mondal R, Farle M and Semisalova A 2022 *Phys. Rev. B* **106** 054428
[22] Titov S V, Dowling W J and Kalmykov Y P 2022 *J. Appl. Phys.* **131** 193901
[23] Anders J, Sait C R J and Horsley S A R 2022 *New J. Phys.* **24** 033020
[24] Cowburn R P, Allwood D A, Xiong G and Cooke M D 2002 *J. Appl. Phys.* **91** 6949
[25] Ono T, Miyajima H, Shigeto K, Mibu K, Hosoito N and Shinjo T 1999 *Science* **284** 468
[26] Berger L 1984 *J. Appl. Phys.* **55** 1954
[27] Berger L 1992 *J. Appl. Phys.* **71** 2721
[28] Grollier J, Boulenc P, Cros V, Hamzic A, Vaur'es A, Fert A and Faini G 2003 *Appl. Phys. Lett.* **83** 509
[29] Kläui M, Vaz C A F, Bland J A C, Wernsdorfer W, Faini G, Cambril E and Heyderman L J 2003 *Appl. Phys. Lett.* **83** 105
[30] Vernier N, Allwood D A, Atkinson D, Cooke M D and Cowburn R P 2004 *Europhys. Lett.* **65** 526
[31] Beach G S D, Knutson C, Nistor C, Tsoi M and Erskine J L 2006 *Phys. Rev. Lett.* **97** 057203
[32] Hayashi M, Thomas L, Rettner C, Moriya R, Bazaliy Y B and Parkin S S P 2007 *Phys. Rev. Lett.* **98** 037204
[33] Schryer N L and Walker L R 1974 *J. Appl. Phys.* **45** 5406
[34] Li Z and Zhang S 2004 *Phys. Rev. Lett.* **92** 207203
[35] Zhang S, Levy P M and Fert A 2002 *Phys. Rev. Lett.* **88** 236601
[36] Allwood D A, Xiong G, Cooke M D, Faulkner C C, Atkinson D, Vernier N and Cowburn R P 2002 *Science* **296** 2003
[37] Yamaguchi A, Ono T, Nasu S, Miyake K, Mibu K and Shinjo T 2004 *Phys. Rev. Lett.* **92** 077205
[38] Tsoi M, Fontana R E and Parkin S S P 2003 *Appl. Phys. Lett.* **83** 2617
[39] Mondal R, Rózsa L, Farle M, Oppeneer P M, Nowak U and Cherkasskii M 2023 *J. Magn. Magn. Mater.* **579** 170830
[40] Winter L, Großenbach S, Nowak U and Rózsa L 2022 *Phys. Rev. B* **106** 214403
[41] Makhfudz I, Hajati Y and Olive E 2022 *Phys. Rev. B* **106** 134415
[42] De A, Lentfert A, Scheuer L, Stadtmüller B, Pirro P, Freymann G v and Aeschlimann M 2025 *Phys. Rev. B* **111** 014432
[43] Rodriguez R, Cherkasskii M, Jiang R, Mondal R, Etesamirad A, Tossounian A, Ivanov B A and Barsukov I 2024 *Phys. Rev. Lett.* **132** 246701
[44] Li Z D, Nan X M and Liu W M 2024 *Phys. E* **159** 115931
[45] Sinova J, Valenzuela S O, Wunderlich J, Back C H and Jungwirth T 2015 *Rev. Mod. Phys.* **87** 1213
[46] Taniguchi T, Grollier J and Stiles M D 2015 *Phys. Rev. Appl.* **3** 044001
[47] Barsukov I, Fu Y, Safranski C, Chen Y J, Youngblood B, Gonçalves A M, Spasova M, Farle M, Katine J A, Kuo C C and Krivorotov I N 2015 *Appl. Phys. Lett.* **106** 192407
[48] Hellman F, Hoffmann A, Tserkovnyak Y, Beach G S, Fullerton E E, Leighton C, MacDonald A H, Ralph D C, Arena D A, Dürr H A and Fischer P 2017 *Rev. Mod. Phys.* **89** 025006
[49] Shao Q, Li P, Liu L, Yang H, Fukami S, Razavi A, Wu H, Wang K, Freimuth F, Mokrousov Y, Stiles M D, Emori S, Hoffmann A, Åkerman J, Roy K, Wang J P, Yang S H, Garello K and Zhang W 2021 *IEEE Trans. Magn.* **57** 1
[50] Safranski C, Montoya E A and Krivorotov I N 2019 *Nat. Nanotechnol.* **14** 27
[51] Montoya E A, Khan A, Safranski C, Smith A and Krivorotov I N 2023 *Commun. Phys.* **6** 184
[52] Etesamirad A, Rodriguez R, Bocanegra J, Verba R, Katine J, Krivorotov I N, Tyberkevych V, Ivanov B and Barsukov I 2021 *ACS Appl. Mater. Interfaces* **13** 20288
[53] Janda T, Roy P E, Otxoa R M, Šobáň Z, Ramsay A, Irvine A C, Trojanek F, Surýnek M, Campion R P, Gallagher B L, Němec P, Jungwirth T and Wunderlich J 2017 *Nat. Commun.* **8** 15226
[54] Gareeva Z and Guslienko K 2023 *Nanomaterials* **13** 461
[55] Tretiakov O A and Abanov Ar 2010 *Phys. Rev. Lett.* **105** 157201
[56] Carva K, Battiato M, Legut D and Oppeneer P M 2013 *Phys. Rev. B* **87** 184425
[57] Kim J W, Vomir M and Bigot J Y 2012 *Phys. Rev. Lett.* **109** 166601
[58] Graves C E, Reid A H, Wang T, Wu B, Jong S De, Vahaplar K, Radu I, Bernstein D P, Messerschmidt M, Müller L and Coffee R 2013 *Nat. Mater.* **12** 293
[59] Iacocca E, Liu T M, Reid A H, Fu Z, Ruta S, Granitzka P W, Jal E, Bonetti S, Gray A X, Graves C E and Kukreja R 2019 *Nat. Commun.* **10** 1756